Search for the rare decay $B \to \pi \, \ell^+\ell^-$

The *BABAR* Collaboration

July 24, 2006

Abstract

We present results of a search for the rare flavor-changing neutral-current decay $B \to \pi\ell^+\ell^-$, based on a data sample corresponding to 209 fb^{-1} of integrated luminosity collected with the *BABAR* detector at the PEP-II B Factory. We reconstruct the four exclusive B decay modes $B^+ \to \pi^+\ell^+\ell^-$ and $B^0 \to \pi^0\ell^+\ell^-$, where ℓ is either an e or μ. We find no evidence for a signal, and we obtain the upper limit at 90% confidence level on the lepton-flavor–averaged branching fraction to be

$$\mathcal{B}(B^+ \to \pi^+\ell^+\ell^-) = 2 \times \frac{\tau_{B^+}}{\tau_{B^0}}\mathcal{B}(B^0 \to \pi^0\ell^+\ell^-) < 7.9 \times 10^{-8}.$$

We also obtain an upper limit at 90% confidence level on the lepton-flavor–violating decay $B \to \pi e\mu$ of

$$\mathcal{B}(B \to \pi e\mu) < 9.8 \times 10^{-8}.$$

Submitted to the 33$^{\mathrm{rd}}$ International Conference on High-Energy Physics, ICHEP 06, 26 July—2 August 2006, Moscow, Russia.

The *BABAR* Collaboration,

B. Aubert, R. Barate, M. Bona, D. Boutigny, F. Couderc, Y. Karyotakis, J. P. Lees, V. Poireau,
V. Tisserand, A. Zghiche

Laboratoire de Physique des Particules, IN2P3/CNRS et Université de Savoie, F-74941 Annecy-Le-Vieux,
France

E. Grauges

Universitat de Barcelona, Facultat de Fisica, Departament ECM, E-08028 Barcelona, Spain

A. Palano

Università di Bari, Dipartimento di Fisica and INFN, I-70126 Bari, Italy

J. C. Chen, N. D. Qi, G. Rong, P. Wang, Y. S. Zhu

Institute of High Energy Physics, Beijing 100039, China

G. Eigen, I. Ofte, B. Stugu

University of Bergen, Institute of Physics, N-5007 Bergen, Norway

G. S. Abrams, M. Battaglia, D. N. Brown, J. Button-Shafer, R. N. Cahn, E. Charles, M. S. Gill,
Y. Groysman, R. G. Jacobsen, J. A. Kadyk, L. T. Kerth, Yu. G. Kolomensky, G. Kukartsev, G. Lynch,
L. M. Mir, T. J. Orimoto, M. Pripstein, N. A. Roe, M. T. Ronan, W. A. Wenzel

Lawrence Berkeley National Laboratory and University of California, Berkeley, California 94720, USA

P. del Amo Sanchez, M. Barrett, K. E. Ford, A. J. Hart, T. J. Harrison, C. M. Hawkes, S. E. Morgan,
A. T. Watson

University of Birmingham, Birmingham, B15 2TT, United Kingdom

T. Held, H. Koch, B. Lewandowski, M. Pelizaeus, K. Peters, T. Schroeder, M. Steinke

Ruhr Universität Bochum, Institut für Experimentalphysik 1, D-44780 Bochum, Germany

J. T. Boyd, J. P. Burke, W. N. Cottingham, D. Walker

University of Bristol, Bristol BS8 1TL, United Kingdom

D. J. Asgeirsson, T. Cuhadar-Donszelmann, B. G. Fulsom, C. Hearty, N. S. Knecht, T. S. Mattison,
J. A. McKenna

University of British Columbia, Vancouver, British Columbia, Canada V6T 1Z1

A. Khan, P. Kyberd, M. Saleem, D. J. Sherwood, L. Teodorescu

Brunel University, Uxbridge, Middlesex UB8 3PH, United Kingdom

V. E. Blinov, A. D. Bukin, V. P. Druzhinin, V. B. Golubev, A. P. Onuchin, S. I. Serednyakov,
Yu. I. Skovpen, E. P. Solodov, K. Yu Todyshev

Budker Institute of Nuclear Physics, Novosibirsk 630090, Russia

D. S. Best, M. Bondioli, M. Bruinsma, M. Chao, S. Curry, I. Eschrich, D. Kirkby, A. J. Lankford, P. Lund,
M. Mandelkern, R. K. Mommsen, W. Roethel, D. P. Stoker

University of California at Irvine, Irvine, California 92697, USA

S. Abachi, C. Buchanan

University of California at Los Angeles, Los Angeles, California 90024, USA

S. D. Foulkes, J. W. Gary, O. Long, B. C. Shen, K. Wang, L. Zhang

University of California at Riverside, Riverside, California 92521, USA

H. K. Hadavand, E. J. Hill, H. P. Paar, S. Rahatlou, V. Sharma

University of California at San Diego, La Jolla, California 92093, USA

J. W. Berryhill, C. Campagnari, A. Cunha, B. Dahmes, T. M. Hong, D. Kovalskyi, J. D. Richman

University of California at Santa Barbara, Santa Barbara, California 93106, USA

T. W. Beck, A. M. Eisner, C. J. Flacco, C. A. Heusch, J. Kroseberg, W. S. Lockman, G. Nesom, T. Schalk,
B. A. Schumm, A. Seiden, P. Spradlin, D. C. Williams, M. G. Wilson

University of California at Santa Cruz, Institute for Particle Physics, Santa Cruz, California 95064, USA

J. Albert, E. Chen, A. Dvoretskii, F. Fang, D. G. Hitlin, I. Narsky, T. Piatenko, F. C. Porter, A. Ryd,
A. Samuel

California Institute of Technology, Pasadena, California 91125, USA

G. Mancinelli, B. T. Meadows, K. Mishra, M. D. Sokoloff

University of Cincinnati, Cincinnati, Ohio 45221, USA

F. Blanc, P. C. Bloom, S. Chen, W. T. Ford, J. F. Hirschauer, A. Kreisel, M. Nagel, U. Nauenberg,
A. Olivas, W. O. Ruddick, J. G. Smith, K. A. Ulmer, S. R. Wagner, J. Zhang

University of Colorado, Boulder, Colorado 80309, USA

A. Chen, E. A. Eckhart, A. Soffer, W. H. Toki, R. J. Wilson, F. Winklmeier, Q. Zeng

Colorado State University, Fort Collins, Colorado 80523, USA

D. D. Altenburg, E. Feltresi, A. Hauke, H. Jasper, J. Merkel, A. Petzold, B. Spaan

Universität Dortmund, Institut für Physik, D-44221 Dortmund, Germany

T. Brandt, V. Klose, H. M. Lacker, W. F. Mader, R. Nogowski, J. Schubert, K. R. Schubert, R. Schwierz,
J. E. Sundermann, A. Volk

Technische Universität Dresden, Institut für Kern- und Teilchenphysik, D-01062 Dresden, Germany

D. Bernard, G. R. Bonneaud, E. Latour, Ch. Thiebaux, M. Verderi

Laboratoire Leprince-Ringuet, CNRS/IN2P3, Ecole Polytechnique, F-91128 Palaiseau, France

P. J. Clark, W. Gradl, F. Muheim, S. Playfer, A. I. Robertson, Y. Xie

University of Edinburgh, Edinburgh EH9 3JZ, United Kingdom

M. Andreotti, D. Bettoni, C. Bozzi, R. Calabrese, G. Cibinetto, E. Luppi, M. Negrini, A. Petrella,
L. Piemontese, E. Prencipe

Università di Ferrara, Dipartimento di Fisica and INFN, I-44100 Ferrara, Italy

F. Anulli, R. Baldini-Ferroli, A. Calcaterra, R. de Sangro, G. Finocchiaro, S. Pacetti, P. Patteri,
I. M. Peruzzi,[1] M. Piccolo, M. Rama, A. Zallo

Laboratori Nazionali di Frascati dell'INFN, I-00044 Frascati, Italy

[1] Also with Università di Perugia, Dipartimento di Fisica, Perugia, Italy

3

A. Buzzo, R. Capra, R. Contri, M. Lo Vetere, M. M. Macri, M. R. Monge, S. Passaggio, C. Patrignani,
E. Robutti, A. Santroni, S. Tosi

Università di Genova, Dipartimento di Fisica and INFN, I-16146 Genova, Italy

G. Brandenburg, K. S. Chaisanguanthum, M. Morii, J. Wu

Harvard University, Cambridge, Massachusetts 02138, USA

R. S. Dubitzky, J. Marks, S. Schenk, U. Uwer

Universität Heidelberg, Physikalisches Institut, Philosophenweg 12, D-69120 Heidelberg, Germany

D. J. Bard, W. Bhimji, D. A. Bowerman, P. D. Dauncey, U. Egede, R. L. Flack, J. A. Nash,
M. B. Nikolich, W. Panduro Vazquez

Imperial College London, London, SW7 2AZ, United Kingdom

P. K. Behera, X. Chai, M. J. Charles, U. Mallik, N. T. Meyer, V. Ziegler

University of Iowa, Iowa City, Iowa 52242, USA

J. Cochran, H. B. Crawley, L. Dong, V. Eyges, W. T. Meyer, S. Prell, E. I. Rosenberg, A. E. Rubin

Iowa State University, Ames, Iowa 50011-3160, USA

A. V. Gritsan

Johns Hopkins University, Baltimore, Maryland 21218, USA

A. G. Denig, M. Fritsch, G. Schott

Universität Karlsruhe, Institut für Experimentelle Kernphysik, D-76021 Karlsruhe, Germany

N. Arnaud, M. Davier, G. Grosdidier, A. Höcker, F. Le Diberder, V. Lepeltier, A. M. Lutz, A. Oyanguren,
S. Pruvot, S. Rodier, P. Roudeau, M. H. Schune, A. Stocchi, W. F. Wang, G. Wormser

*Laboratoire de l'Accélérateur Linéaire, IN2P3/CNRS et Université Paris-Sud 11, Centre Scientifique
d'Orsay, B.P. 34, F-91898 ORSAY Cedex, France*

C. H. Cheng, D. J. Lange, D. M. Wright

Lawrence Livermore National Laboratory, Livermore, California 94550, USA

C. A. Chavez, I. J. Forster, J. R. Fry, E. Gabathuler, R. Gamet, K. A. George, D. E. Hutchcroft,
D. J. Payne, K. C. Schofield, C. Touramanis

University of Liverpool, Liverpool L69 7ZE, United Kingdom

A. J. Bevan, F. Di Lodovico, W. Menges, R. Sacco

Queen Mary, University of London, E1 4NS, United Kingdom

G. Cowan, H. U. Flaecher, D. A. Hopkins, P. S. Jackson, T. R. McMahon, S. Ricciardi, F. Salvatore,
A. C. Wren

*University of London, Royal Holloway and Bedford New College, Egham, Surrey TW20 0EX, United
Kingdom*

D. N. Brown, C. L. Davis

University of Louisville, Louisville, Kentucky 40292, USA

J. Allison, N. R. Barlow, R. J. Barlow, Y. M. Chia, C. L. Edgar, G. D. Lafferty, M. T. Naisbit,
J. C. Williams, J. I. Yi

University of Manchester, Manchester M13 9PL, United Kingdom

C. Chen, W. D. Hulsbergen, A. Jawahery, C. K. Lae, D. A. Roberts, G. Simi

University of Maryland, College Park, Maryland 20742, USA

G. Blaylock, C. Dallapiccola, S. S. Hertzbach, X. Li, T. B. Moore, S. Saremi, H. Staengle

University of Massachusetts, Amherst, Massachusetts 01003, USA

R. Cowan, G. Sciolla, S. J. Sekula, M. Spitznagel, F. Taylor, R. K. Yamamoto

*Massachusetts Institute of Technology, Laboratory for Nuclear Science, Cambridge, Massachusetts 02139,
USA*

H. Kim, S. E. Mclachlin, P. M. Patel, S. H. Robertson

McGill University, Montréal, Québec, Canada H3A 2T8

A. Lazzaro, V. Lombardo, F. Palombo

Università di Milano, Dipartimento di Fisica and INFN, I-20133 Milano, Italy

J. M. Bauer, L. Cremaldi, V. Eschenburg, R. Godang, R. Kroeger, D. A. Sanders, D. J. Summers,
H. W. Zhao

University of Mississippi, University, Mississippi 38677, USA

S. Brunet, D. Côté, M. Simard, P. Taras, F. B. Viaud

Université de Montréal, Physique des Particules, Montréal, Québec, Canada H3C 3J7

H. Nicholson

Mount Holyoke College, South Hadley, Massachusetts 01075, USA

N. Cavallo,[2] G. De Nardo, F. Fabozzi,[3] C. Gatto, L. Lista, D. Monorchio, P. Paolucci, D. Piccolo,
C. Sciacca

Università di Napoli Federico II, Dipartimento di Scienze Fisiche and INFN, I-80126, Napoli, Italy

M. A. Baak, G. Raven, H. L. Snoek

*NIKHEF, National Institute for Nuclear Physics and High Energy Physics, NL-1009 DB Amsterdam, The
Netherlands*

C. P. Jessop, J. M. LoSecco

University of Notre Dame, Notre Dame, Indiana 46556, USA

T. Allmendinger, G. Benelli, L. A. Corwin, K. K. Gan, K. Honscheid, D. Hufnagel, P. D. Jackson,
H. Kagan, R. Kass, A. M. Rahimi, J. J. Regensburger, R. Ter-Antonyan, Q. K. Wong

Ohio State University, Columbus, Ohio 43210, USA

N. L. Blount, J. Brau, R. Frey, O. Igonkina, J. A. Kolb, M. Lu, R. Rahmat, N. B. Sinev, D. Strom,
J. Strube, E. Torrence

University of Oregon, Eugene, Oregon 97403, USA

---

[2]Also with Università della Basilicata, Potenza, Italy
[3]Also with Università della Basilicata, Potenza, Italy

A. Gaz, M. Margoni, M. Morandin, A. Pompili, M. Posocco, M. Rotondo, F. Simonetto, R. Stroili, C. Voci

Università di Padova, Dipartimento di Fisica and INFN, I-35131 Padova, Italy

M. Benayoun, H. Briand, J. Chauveau, P. David, L. Del Buono, Ch. de la Vaissière, O. Hamon, B. L. Hartfiel, M. J. J. John, Ph. Leruste, J. Malclès, J. Ocariz, L. Roos, G. Therin

Laboratoire de Physique Nucléaire et de Hautes Energies, IN2P3/CNRS, Université Pierre et Marie Curie-Paris6, Université Denis Diderot-Paris7, F-75252 Paris, France

L. Gladney, J. Panetta

University of Pennsylvania, Philadelphia, Pennsylvania 19104, USA

M. Biasini, R. Covarelli

Università di Perugia, Dipartimento di Fisica and INFN, I-06100 Perugia, Italy

C. Angelini, G. Batignani, S. Bettarini, F. Bucci, G. Calderini, M. Carpinelli, R. Cenci, F. Forti, M. A. Giorgi, A. Lusiani, G. Marchiori, M. A. Mazur, M. Morganti, N. Neri, E. Paoloni, G. Rizzo, J. J. Walsh

Università di Pisa, Dipartimento di Fisica, Scuola Normale Superiore and INFN, I-56127 Pisa, Italy

M. Haire, D. Judd, D. E. Wagoner

Prairie View A&M University, Prairie View, Texas 77446, USA

J. Biesiada, N. Danielson, P. Elmer, Y. P. Lau, C. Lu, J. Olsen, A. J. S. Smith, A. V. Telnov

Princeton University, Princeton, New Jersey 08544, USA

F. Bellini, G. Cavoto, A. D'Orazio, D. del Re, E. Di Marco, R. Faccini, F. Ferrarotto, F. Ferroni, M. Gaspero, L. Li Gioi, M. A. Mazzoni, S. Morganti, G. Piredda, F. Polci, F. Safai Tehrani, C. Voena

Università di Roma La Sapienza, Dipartimento di Fisica and INFN, I-00185 Roma, Italy

M. Ebert, H. Schröder, R. Waldi

Universität Rostock, D-18051 Rostock, Germany

T. Adye, N. De Groot, B. Franek, E. O. Olaiya, F. F. Wilson

Rutherford Appleton Laboratory, Chilton, Didcot, Oxon, OX11 0QX, United Kingdom

R. Aleksan, S. Emery, A. Gaidot, S. F. Ganzhur, G. Hamel de Monchenault, W. Kozanecki, M. Legendre, G. Vasseur, Ch. Yèche, M. Zito

DSM/Dapnia, CEA/Saclay, F-91191 Gif-sur-Yvette, France

X. R. Chen, H. Liu, W. Park, M. V. Purohit, J. R. Wilson

University of South Carolina, Columbia, South Carolina 29208, USA

M. T. Allen, D. Aston, R. Bartoldus, P. Bechtle, N. Berger, R. Claus, J. P. Coleman, M. R. Convery, M. Cristinziani, J. C. Dingfelder, J. Dorfan, G. P. Dubois-Felsmann, D. Dujmic, W. Dunwoodie, R. C. Field, T. Glanzman, S. J. Gowdy, M. T. Graham, P. Grenier,[4] V. Halyo, C. Hast, T. Hryn'ova, W. R. Innes, M. H. Kelsey, P. Kim, D. W. G. S. Leith, S. Li, S. Luitz, V. Luth, H. L. Lynch, D. B. MacFarlane, H. Marsiske, R. Messner, D. R. Muller, C. P. O'Grady, V. E. Ozcan, A. Perazzo, M. Perl, T. Pulliam, B. N. Ratcliff, A. Roodman, A. A. Salnikov, R. H. Schindler, J. Schwiening, A. Snyder, J. Stelzer, D. Su, M. K. Sullivan, K. Suzuki, S. K. Swain, J. M. Thompson, J. Va'vra, N. van

---

[4]Also at Laboratoire de Physique Corpusculaire, Clermont-Ferrand, France

Bakel, M. Weaver, A. J. R. Weinstein, W. J. Wisniewski, M. Wittgen, D. H. Wright, A. K. Yarritu, K. Yi,
C. C. Young

Stanford Linear Accelerator Center, Stanford, California 94309, USA

P. R. Burchat, A. J. Edwards, S. A. Majewski, B. A. Petersen, C. Roat, L. Wilden

Stanford University, Stanford, California 94305-4060, USA

S. Ahmed, M. S. Alam, R. Bula, J. A. Ernst, V. Jain, B. Pan, M. A. Saeed, F. R. Wappler, S. B. Zain

State University of New York, Albany, New York 12222, USA

W. Bugg, M. Krishnamurthy, S. M. Spanier

University of Tennessee, Knoxville, Tennessee 37996, USA

R. Eckmann, J. L. Ritchie, A. Satpathy, C. J. Schilling, R. F. Schwitters

University of Texas at Austin, Austin, Texas 78712, USA

J. M. Izen, X. C. Lou, S. Ye

University of Texas at Dallas, Richardson, Texas 75083, USA

F. Bianchi, F. Gallo, D. Gamba

Università di Torino, Dipartimento di Fisica Sperimentale and INFN, I-10125 Torino, Italy

M. Bomben, L. Bosisio, C. Cartaro, F. Cossutti, G. Della Ricca, S. Dittongo, L. Lanceri, L. Vitale

Università di Trieste, Dipartimento di Fisica and INFN, I-34127 Trieste, Italy

V. Azzolini, N. Lopez-March, F. Martinez-Vidal

IFIC, Universitat de Valencia-CSIC, E-46071 Valencia, Spain

Sw. Banerjee, B. Bhuyan, C. M. Brown, D. Fortin, K. Hamano, R. Kowalewski, I. M. Nugent, J. M. Roney,
R. J. Sobie

University of Victoria, Victoria, British Columbia, Canada V8W 3P6

J. J. Back, P. F. Harrison, T. E. Latham, G. B. Mohanty, M. Pappagallo

Department of Physics, University of Warwick, Coventry CV4 7AL, United Kingdom

H. R. Band, X. Chen, B. Cheng, S. Dasu, M. Datta, K. T. Flood, J. J. Hollar, P. E. Kutter, B. Mellado,
A. Mihalyi, Y. Pan, M. Pierini, R. Prepost, S. L. Wu, Z. Yu

University of Wisconsin, Madison, Wisconsin 53706, USA

H. Neal

Yale University, New Haven, Connecticut 06511, USA

1 Introduction

The decays $B \to \pi \ell^+ \ell^-$, where $\ell^+ \ell^-$ is either an $e^+ e^-$ or $\mu^+ \mu^-$ pair, are the simplest manifestations of $b \to d\ell^+\ell^-$ flavor-changing neutral currents (FCNC). In the Standard Model (SM), these decays are forbidden at tree level and can only occur at greatly suppressed rates through higher-order processes. At lowest order in the electroweak couplings, three amplitudes contribute: (1) a photon penguin, (2) a Z penguin, and (3) a W^+W^- box diagram (Fig. 1). Since these decays proceed via weakly-interacting particles with virtual energies near the electroweak scale, they provide a promising means to search for effects from new flavor-changing interactions. Such effects are predicted in a wide variety of models, usually in the context of the similar FCNC $b \to s\ell^+\ell^-$ [1–5]. If there exists non-trivial flavor violation in the new interactions, $b \to d\ell^+\ell^-$ can also exhibit large observable effects, independent of the experimental constraints on $b \to s\ell^+\ell^-$ [6,7].

In the Standard Model, the $b \to d$ FCNC decay rate is suppressed relative to $b \to s$ by a ratio of Cabibbo-Kobayashi-Maskawa matrix elements $|V_{td}/V_{ts}|^2$, making them especially rare processes which challenge the sensitivity of the B factories. The chief experimental constraint on $\Delta B = 1$ $b \to d$ FCNC decays comes from recent measurements of the exclusive decays $B \to \rho\gamma$ and $B \to \omega\gamma$ [8], which constrain the photon penguin decay rate to agree with SM predictions with an experimental precision of 30%. The additional $b \to d$ electroweak amplitudes present in $b \to d\ell^+\ell^-$ are weakly constrained experimentally from older measurements [9]. A recent SM prediction [10] for the $B^+ \to \pi^+\ell^+\ell^-$ branching fraction is based on an operator product expansion combined with $B \to \pi$ form factor predictions from light-cone QCD sum rules; the predicted branching fraction is 3.3×10^{-8} with an uncertainty of about 30%. The $B^0 \to \pi^0\ell^+\ell^-$ branching fraction is related to the charged mode by isospin symmetry; accounting for the difference in charged and neutral B meson lifetimes, the branching fraction is given by $\frac{1}{2} \times \tau_{B^0}/\tau_{B^+} \times \mathcal{B}(B^+ \to \pi^+\ell^+\ell^-)$.
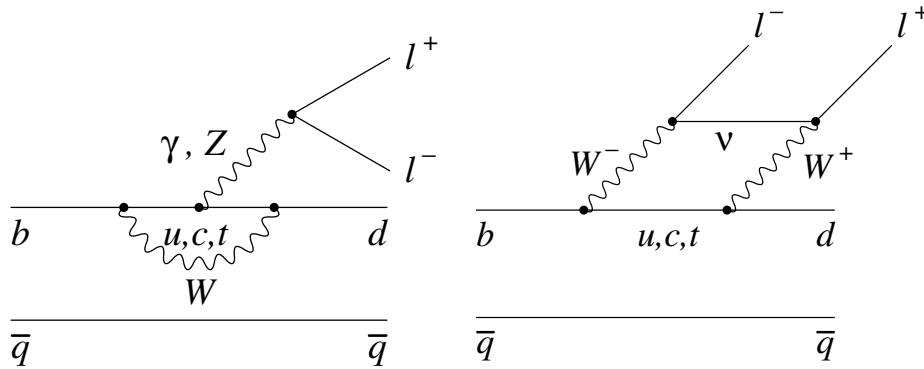

Figure 1: Standard Model diagrams for the decays $B \to \pi\ell^+\ell^-$. For the photon or Z penguin diagrams on the left, boson emission can occur on any of the b, t, c, u, d, or W lines.

We also perform a search for the lepton-flavor violating decay $B \to \pi e^{\pm}\mu^{\mp}$ which can occur in some models beyond the Standard Model, such as theories involving leptoquarks [5]. Earlier searches [11] for these modes have yielded no such events.

2 The BABAR Detector and Dataset

The data used in this analysis were collected with the BABAR detector at the PEP-II storage ring located at the Stanford Linear Accelerator Center. The data sample comprises 208.9 fb^{-1} recorded near the peak of the $\Upsilon(4S)$ resonance, yielding $(230.1 \pm 2.5) \times 10^6$ $B\overline{B}$ decays, and an off-resonance sample of 21.5 fb^{-1} which is used to study continuum background.

The BABAR detector is described in detail elsewhere [12]. Its most important capabilities for this study are charged-particle tracking and momentum measurement, charged π/K separation, and lepton identification. Charged particle tracking is provided by a five-layer silicon vertex tracker (SVT) and a 40-layer drift chamber (DCH). The DIRC, a Cherenkov ring-imaging particle-identification system, is used to identify charged kaons and pions. Electrons are identified using the electromagnetic calorimeter (EMC), which comprises 6580 thallium-doped CsI crystals. These systems are mounted inside a 1.5 T solenoidal superconducting magnet. Muons are identified in the instrumented flux return (IFR), in which resistive plate chambers are interleaved with the iron plates of the magnet flux return.

3 Analysis Method

3.1 Event Selection

We select events that include two oppositely charged leptons (e^+e^-, $\mu^+\mu^-$ and $e^\pm\mu^\mp$) as well as a pion (either a $\pi^\pm$ track or a π^0 meson decaying to $\gamma\gamma$). The analysis faces the experimental challenge of isolating a very rare B-meson decay from background due to random combinations of particles in generic $e^+e^- \to \Upsilon(4S) \to B\overline{B}$ and continuum $e^+e^- \to q\bar{q}$ events ($q\bar{q}$ being a pair of $u,d,s,$ or c quarks), and there is a great abundance of pions and leptons in all of these events. We use stringent particle identification and a multivariate algorithm to reduce this background. Another type of background comes from events that have signal-like features. The main contributions to such backgrounds are from B-mesons decaying to charmonium states (e.g. $B \to J/\psi\ \pi$ where the J/ψ decays to two leptons) or B-mesons decaying to three hadrons (e.g. $B \to D\pi$ with $D \to K\pi$) where two of the hadrons pass the muon selection. In addition, there is background from the $b \to s\ell^+\ell^-$ penguin decay $B \to K\ \ell^+\ell^-$, which has a branching fraction about one order of magnitude larger than expected for $B \to \pi\ \ell^+\ell^-$ [6, 10]. These events have a reconstructed B energy lower than expected for signal events and are also very efficiently reduced by information from the DIRC subdetector.

Electrons are required to have a momentum $p > 0.3$ GeV/c and are identified combining information from the EMC, DIRC, and DCH. Photons with $E > 30$ MeV that lie within an angular region of 50 mrad in the azimuth angle ϕ and 35 mrad in the polar angle θ of the initial electron track direction are combined with electron candidates in order to recover energy lost by bremsstrahlung. We suppress backgrounds due to photon conversions in the $B \to \pi\ e^+e^-$ channels by removing e^+e^- pairs with invariant mass less than 30 MeV/c^2. Muons with momentum $p > 0.7$ GeV/c are identified with a neural network algorithm using information from the IFR and the EMC.

The lepton pairs are combined with a charged or neutral pion candidate to reconstruct a B meson. Charged pion candidates are tracks with specific ionization (dE/dx) and Cherenkov angle consistent with a pion. A likelihood algorithm based on this information reduces fake rates from kaons down to about $1 - 5\%$ depending on the track momentum. Neutral pion candidates are identified as pairs of neutral-energy deposits in the EMC, each with an energy greater than 50 MeV in the laboratory frame. The invariant mass of the pair is calculated under the assumption

9

that the photons originate from the $\ell^+\ell^-$ vertex, and is required to satisfy $115 < m_{\gamma\gamma} < 150$ MeV/c^2.

Correctly reconstructed B signal decays produce narrow peaks in the distributions of two kinematic variables, which can be used to extract the signal and background yields. For a candidate system of B daughter particles with masses m_i and three-momenta $\mathbf{p}_i^*$ in the $\Upsilon(4S)$ center-of-mass (CM) frame, we define $m_{\mathrm{ES}} = \sqrt{E_{\mathrm{b}}^{*2} - |\sum_i \mathbf{p}_i^*|^2}$ and $\Delta E = \sum_i \sqrt{m_i^2 + \mathbf{p}_i^{*2}} - E_{\mathrm{b}}^*$, where E_{b}^* is the beam energy in the CM frame. For signal events, the m_{ES} distribution peaks at the B meson mass and has a width $\sigma_{m_{\mathrm{ES}}} \approx 2.5$ MeV/c^2, and the ΔE distribution peaks near zero, with a typical width $\sigma_{\Delta E} \approx 20$ MeV. The mean and width of the m_{ES} and ΔE distributions are determined separately for e^+e^- and $\mu^+\mu^-$ modes using data control samples. For events reconstructed as $e^\pm\mu^\mp$ we assume the same width and mean as for the e^+e^- modes.

We define two kinematic regions in terms of m_{ES} and ΔE for signal extraction purposes. The signal region is defined to be within 2σ of the expected mean of the peak in m_{ES} and ΔE. The values are given in Table 1. A 2σ signal region width was found to be close to optimal for both the $S/\sqrt{S+B}$ and $S/\sqrt{B}$ figure of merit, where S and B are the number of signal and background events expected based on Monte Carlo simulations.

Table 1: Boundary values defining the signal region for each $B \to \pi \ell^+ \ell^-$ mode. The boundaries used in the $B^+ \to \pi^+ e\mu$ and $B^0 \to \pi^0 e\mu$ modes are the same as for $B^+ \to \pi^+ e^+ e^-$ and $B^0 \to \pi^0 e^+ e^-$ modes, respectively.

mode	m_{ES} low [GeV/c^2]	m_{ES} high [GeV/c^2]	ΔE low [MeV]	ΔE high [MeV]
$B^+ \to \pi^+ e^+ e^-$	5.2748	5.2847	-53.6	37.4
$B^0 \to \pi^0 e^+ e^-$	5.2767	5.2839	-115.0	82.5
$B^+ \to \pi^+ \mu^+ \mu^-$	5.2749	5.2847	-42.0	35.0
$B^0 \to \pi^0 \mu^+ \mu^-$	5.2764	5.2836	-87.4	68.0

We blind ourselves from inspecting the signal region, and also a broader region in the m_{ES}–ΔE plane, until all selection criteria are optimized and control samples are checked. The broader region is used to determine the number of background events from an unbinned maximum likelihood fit directly from the data. This fit region is defined as $5.2 \,\mathrm{GeV}/c^2 < m_{\mathrm{ES}}$ and $|\Delta E| < 0.25 \,\mathrm{GeV}$.

Backgrounds arise from three main sources: random combinations of particles from $q\bar{q}$ and $\tau^+\tau^-$ events produced in the continuum, random combinations of particles from $\Upsilon(4S) \to B\overline{B}$ decays, and B decays to topologies similar to the signal modes. The first two, "combinatorial", backgrounds typically arise from pairs of semileptonic decays and produce broad distributions in m_{ES} and ΔE compared to the signal. The third source arises from modes which have shapes similar to the signal, such as $B \to J/\psi\pi$, with $J/\psi \to \ell^+\ell^-$, or $B \to K\pi\pi$, with kaons or pions misidentified as muons. All selection criteria are optimized with GEANT4 [13] simulated data, independent data control samples or with data samples outside the full fit region.

We suppress combinatorial background from continuum processes by selecting events with high values in a Fisher discriminant [14] constructed as a linear combination of variables with coefficients optimized to distinguish between signal and background. The variables (defined in the CM frame) are (1) the ratio of second- to zeroth-order Fox-Wolfram moments [15] for the event, computed using all charged tracks and neutral energy clusters; (2) the absolute value of the angle between the thrust axis of the B candidate and that of the remaining particles in the event; (3) the production

angle θ_B of the B candidate with respect to the beam axis; and (4) the ratio of second- to zeroth-order Legendre moments [16] for the event, computed using all charged tracks and neutral energy clusters. These variables exploit the difference between the relatively spherical track distribution in $B\bar{B}$ events and the jet-like structure of continuum events.

We suppress combinatorial backgrounds from $B\overline{B}$ events by selecting events with high values in a likelihood function constructed from (1) the missing energy of the event, computed from all charged tracks and neutral energy clusters; (2) the vertex fit probability of all tracks from the B candidate; (3) the vertex fit probability of the two leptons; and (4) the angle θ_B of the B candidate with respect to the beam axis in the direction of the negative electron beam. Missing energy provides the strongest suppression of combinatorial $B\bar{B}$ background events, which typically contain energetic neutrinos from at least two semileptonic B or D meson decays.

Both the continuum and $B\bar{B}$ suppression discriminants are constructed separately for each e^+e^- and $\mu^+\mu^-$ mode. Parameters of the Fisher discriminant have been determined from simulated signal events and a data control sample selected below the $\Upsilon(4S)$ energy. The likelihood function parameters have been determined from simulated signal events and simulated generic $B\overline{B}$ events to separate signal events from other types of $B\overline{B}$ backgrounds. For each reconstruction mode, the required minimum values of the Fisher and likelihood functions are optimized simultaneously by maximizing $S/\sqrt{S+B}$, where S is the expected signal yield in the signal region, and B is the expected background yield in the signal region based on a combination of generic $B\overline{B}$ and continuum Monte Carlo simulated events. The background yields are extracted from a two-dimensional, unbinned, maximum-likelihood fit to the simulated events in the fit region. A branching fraction of $\mathcal{B}(B \to \pi\ell\ell)$ of 3.3×10^{-8} [10] is assumed as the signal estimate. The optimal selection criteria do not change significantly if we alternatively optimize for $S/\sqrt{B}$. For the $\pi e^\pm \mu^\mp$ sample we use the same parameters and optimal selection points as found for the e^+e^- modes.

The most prominent backgrounds that peak in the signal region are B decays to charmonium: $B \to J/\psi\ \pi$ (with $J/\psi \to \ell^+\ell^-$). The more abundant $B \to J/\psi\ K$ decay also contributes as background to $B \to \pi\ \ell^+\ell^-$. This latter background is strongly suppressed by particle identification requirements, and such events typically have a reconstructed B energy which is lower than expected for our signal mode, so that most of these events are outside the signal region for $B \to \pi\ \ell^+\ell^-$. Similarly, B decays to $\psi(2S)\pi(K)$ final states contribute with a peaking background component. We exclude dilepton pairs with dilepton invariant mass $m_{\ell^+\ell^-}$ consistent with the J/ψ mass ($2.90 < m_{e^+e^-} < 3.20$ GeV/c^2 and $3.00 < m_{\mu^+\mu^-} < 3.20$ GeV/c^2) or with the $\psi(2S)$ mass ($3.60 < m_{\ell^+\ell^-} < 3.75$ GeV/c^2). This veto is also applied to $m_{e^+e^-}$ computed without bremsstrahlung photon recovery. When a lepton radiates or is mismeasured, $m_{\ell^+\ell^-}$ can shift away from the charmonium mass, while ΔE shifts in a correlated manner. Therefore, we apply an additional veto with $m_{\ell^+\ell^-}$ veto regions defined as a linear function of ΔE. By extending the veto region this way, we remove nearly all charmonium events from the fit region and simplify the shape of the background PDF in the fit region. For $e^\pm \mu^\mp$ the charmonium vetoes are defined to be the same as for the e^+e^- modes.

The charmonium events removed by these vetoes are otherwise kinematically similar to signal events. These events therefore serve as copious control samples for studying signal shapes, selection efficiencies, and systematic errors. Figure 2 shows the distributions of the two background rejection variables for the $B^+ \to J/\psi\ K^+$ control sample. This sample is selected with identical requirements as our signal sample, except the J/ψ veto has been reversed and the hadron track passes kaon identification. The figure also shows the distributions for simulated $B^+ \to J/\psi; K^+$ events and the simulations agree well with the data. We use this sample to measure the efficiency

11

and bound systematic uncertainties of lepton identification, Fisher discriminant, and B likelihood requirements.

In addition to studying the efficiencies using the charmonium control sample, we measure the branching fractions of $\mathcal{B}(B \to J/\psi \, \pi)$ using $B \to \pi \ell^+ \ell^-$ candidates which fail the charmonium veto. The measured branching fractions are consistent with the world averages for these modes [17].
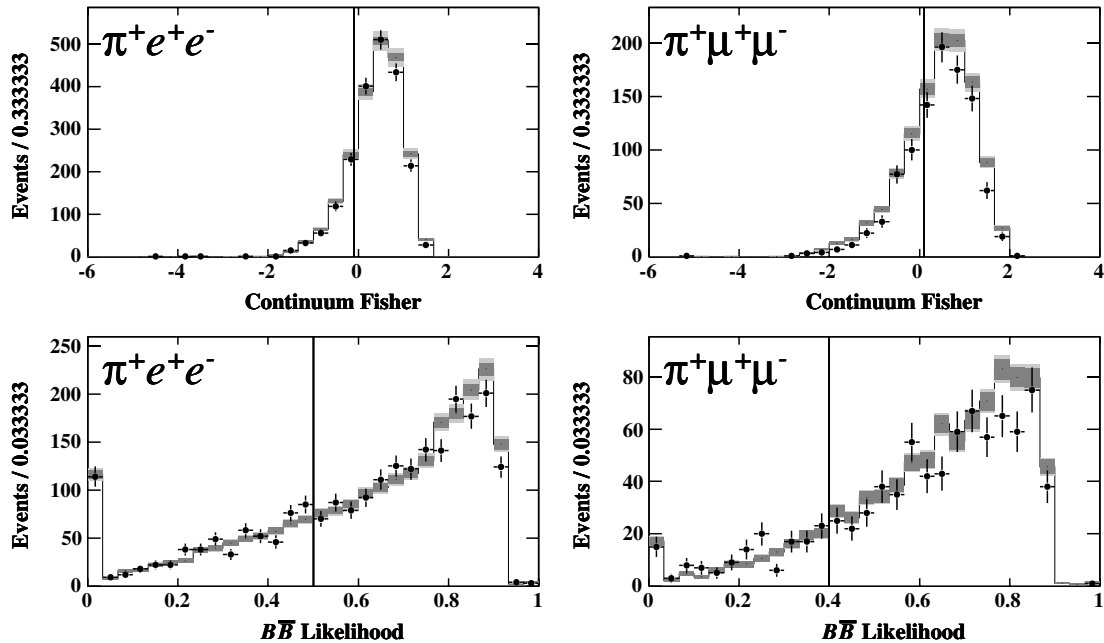

Figure 2: Distribution of the Fisher and likelihood variables in the $J/\psi K^+$ control sample. The black points are *BABAR* data events and the histograms show comparison with simulated events, with statistical and systematic uncertainties shown in the dark and light gray bands, respectively. The vertical lines indicate the optimal cut values for each variable. Our event selection corresponds to events to the right of the vertical line.

In modes with two muons in the final state, where the probability for a hadron to be misidentified as a muon can be as high as a few percent, background from hadronic B-decays like $B \to D\pi$ with $D \to \pi\pi$ or $D \to K\pi$ is significant. These events are suppressed by vetoing events where the $B \to \pi \, \ell^+ \ell^-$ kinematics are consistent with those of a hadronic D decay. We evaluate the $m_{\ell^+\ell^-}$ and $m_{\pi\ell}$ invariant masses with π or K mass hypotheses on the tracks in all combinations corresponding to known D-meson decay modes; we veto those events which have two oppositely-charged tracks with an invariant mass within the range $1.84 - 1.89$ GeV/c^2, or events which have a neutral pion and charged track combination with an invariant mass within the range $1.79 - 1.94$ GeV/c^2.

If more than one charged B-meson candidate remain after all selection requirements have been applied, we select the candidate for which the pion has the greatest number of hits in the SVT tracking detector. If more than one neutral B-meson candidate remain, we select the first one that appears in our data sample (*i.e.* a random candidate); the efficiency of this choice is nearly identical to choosing based on the reconstructed π^0 mass. These criteria are chosen in favor of methods using kinematic information to avoid any bias due to possible correlations with the signal

extraction variables m_{ES} and ΔE. More than one B candidate per event occurs in about 13-15% of charged-B signal events and 35-60% of neutral-B signal events, and typically the multiple candidates are due to more than one possible π candidate. For the $e^{\pm}\mu^{\mp}$ modes more than one B candidate occurs in about 5% of events.

3.2 Signal Extraction and Background Estimate

The signal is extracted by counting events in the signal region. An upper limit on the branching fraction $\mathcal{B}(B \rightarrow \pi\, \ell^+\ell^-)$ is determined from the observed number of events and the expected number of background events in this region. We determine the background expectation before inspecting the signal region.

The number of combinatorial background events is extracted by performing a two-dimensional unbinned maximum-likelihood fit to m_{ES} and ΔE in the region $m_{\mathrm{ES}} < 5.2724$ GeV/c^2 and $|\Delta E| < 0.25$ GeV. The background probability distribution function (PDF) is modeled as the product of an ARGUS function [18] for m_{ES} and an exponential function for ΔE. The slopes and normalization of these functions are floating in the fit, while the endpoint of the ARGUS function is fixed to 5.290 GeV/c^2. The PDF is extrapolated into the signal region (up to $m_{\mathrm{ES}} < 5.290$ GeV/c^2) and the expected number of background events in the signal region is obtained from integrating the PDF over the signal region. The expected number of combinatorial background events is given in Table 2.

We estimate the remaining hadronic B background from a data control sample of mainly $B \rightarrow \pi\pi\pi$ and $B \rightarrow K\pi\pi$ events. In the signal sample these events are highly suppressed by the lepton identification criteria. For the hadronic control sample we select events where the charged tracks fail electron and muon identification, except that for data reduction purposes we require that one track (and only one) pass a looser muon identification criteria which still has a high hadron fake rate. This selects a sample of predominantly hadronic events. These hadronic events are further weighted by their probability to pass the signal-selection muon identification, by weighting each track with a probability depending on its particle type hypothesis, momentum and direction. These track-by-track probabilities are determined from data control samples specifically selected to study particle identification efficiencies. Looking at events with a ΔE consistent with a correctly reconstructed B-meson, we fit the weighted m_{ES} distribution for these events to obtain the expected number of hadronic peaking background events in the signal region. We estimate a background of 0.06 ± 0.05 events in the $\pi^+\mu^+\mu^-$ channel and 0.11 ± 0.04 events in the $\pi^0\mu^+\mu^-$ channel, where the dominant uncertainty is the statistical uncertainty of the fit. We expect no such peaking background in the electron modes or in the $e\mu$ modes.

B-meson decays to $K\,\ell^+\ell^-$ and $\rho\,\ell^+\ell^-$ in the final state are the only other major peaking background components expected. The former shift toward lower reconstructed B energy and are mostly outside the 2σ signal region. This is the sole largest peaking background component for the $\pi^+e^+e^-$ mode. The latter contribute even less, since the reconstructed B in these cases is missing a pion. These estimates are based on high-statistics samples of simulated events. In total, we estimate the number of peaking background events from leptonic events to range from 0.07 ± 0.02 events for the $\pi^+e^+e^-$ mode down to 0.02 ± 0.01 events for the $\pi^0\mu^+\mu^-$ mode. No leptonic peaking background is expected in the $e\mu$ modes.

After the vetoes of $B \rightarrow J/\psi\,\pi(K)$ and $B \rightarrow \psi(2S)\,\pi(K)$ decays, no remaining background from these are expected, as estimated from Monte Carlo simulations.

Table 2 summarizes the number of background events expected in the signal region and the systematic uncertainties associated with these estimates.

Table 2: Estimated number of background events and their associated systematic uncertainties. The m_{ES}-ΔE fit uncertainties are evaluated by varying the parameters of the fit by $\pm 1\sigma$, and the m_{ES}-ΔE correlations and ΔE shape uncertainties are evaluated from using alternative probability density functions. Estimates and systematics from the peaking background are based on Monte Carlo and control sample studies.

Systematic	$\pi^+ e^+ e^-$	$\pi^0 e^+ e^-$	$\pi^+ \mu^+ \mu^-$	$\pi^0 \mu^+ \mu^-$	$\pi^+ e\mu$	$\pi^0 e\mu$
m_{ES}-ΔE fit	0.89 ± 0.31	0.43 ± 0.21	0.86 ± 0.24	0.22 ± 0.18	1.48 ± 0.33	1.13 ± 0.40
m_{ES}-ΔE correlations	± 0.02	± 0.03	± 0.06	± 0.03	± 0.17	± 0.05
ΔE shape	± 0.03	± 0.03	± 0.15	± 0.02	± 0.31	± 0.24
Leptonic peaking bkg.	0.07 ± 0.02	0.03 ± 0.01	0.04 ± 0.01	0.02 ± 0.01	0.00 ± 0.00	0.00 ± 0.00
Hadronic peaking bkg.	0.00 ± 0.00	0.00 ± 0.00	0.06 ± 0.05	0.11 ± 0.04	0.00 ± 0.00	0.00 ± 0.00
Total	0.96 ± 0.32	0.46 ± 0.22	0.96 ± 0.30	0.35 ± 0.19	1.48 ± 0.48	1.13 ± 0.47

4   Systematic Uncertainties

In evaluating systematic uncertainties for the branching fractions, we consider both the uncertainties that affect the signal efficiency estimate, and uncertainties arising from the background estimate. Table 3 lists the systematic uncertainties considered for the signal efficiency. Sources of uncertainties that affect the efficiency are: charged-particle tracking efficiency (0.8% per lepton, 1.4% per charged hadron), charged-particle identification (0.7% per electron pair, 1.9% per muon pair, 0.5% per pion), the continuum background and $B\overline{B}$ suppression selection (1.4%–1.9% depending on the mode), and signal simulation statistics (0.1%). The estimated number of $B\overline{B}$ events in our data sample has an uncertainty of 1.1%. An additional systematic uncertainty for the efficiency results from the choice of form factor model, which alters the q^2 distribution of the signal. We take this uncertainty to be the same as found in [6], which uses the same signal model as this analysis.

Finally, the uncertainties due to the signal efficiency of the m_{ES} and ΔE selection requirements are determined from the measured mean and width of these distributions in charmonium control samples. For $B^+ \to \pi^+ \ell^+ \ell^-$, we use samples of $B \to J/\psi K^+$ events, in which the mean and width are precisely bounded; for $B^0 \to \pi^0 \ell^+ \ell^-$, we use samples of $B \to J/\psi \pi^0$ events, which have limited statistics and introduce a total systematic uncertainty of 7%. For the electron modes, we allow for a larger or smaller bremsstrahlung tail in the ΔE distribution, introducing a systematic uncertainty of 1-2%. The total systematic uncertainty of the signal efficiency is 5% for $B^+ \to \pi^+ \ell^+ \ell^-$ and 9% for $B^0 \to \pi^0 \ell^+ \ell^-$.

Systematic uncertainties for the estimated backgrounds arise from two sources: uncertainties of the maximum likelihood fit which determines the combinatorial background, and uncertainties of the peaking background estimates. Table 2 summarizes the sources of background systematics. In the maximum likelihood fit to the region defined by $5.2 < m_{\mathrm{ES}} < 5.2724\,\mathrm{GeV}/c^2$ and $|\Delta E| < 0.25\,\mathrm{GeV}$, the uncertainty of the extrapolated signal box yield is determined from the induced change due to $\pm 1\sigma$ variations in the fit region yield, the slope parameter in the m_{ES} PDF, and the exponent of the ΔE PDF. We also consider the effect of using different PDF parameterizations on the background estimates, and use the computed differences to bound a systematic uncertainty. We fit a PDF which is correlated in m_{ES} and ΔE via a linear ΔE dependence in m_{ES} slope parameter. We also estimate background from fits for which the ΔE PDF is a linear or quadratic polynomial. These alternative fits result in differences in estimated background generally smaller than the uncertainties

Table 3: The sources of systematic uncertainty in signal efficiency (%) considered for $\pi\,\ell^+\ell^-$ decays.

Systematic	$\pi^+e^+e^-$	$\pi^0e^+e^-$	$\pi^+\mu^+\mu^-$	$\pi^0\mu^+\mu^-$	$\pi^+e\mu$	$\pi^0e\mu$
Trk eff.	±3.0	±1.6	±3.0	±1.6	±3.0	±1.6
Electron ID	±0.7	±0.7			±0.4	±0.4
Muon ID			±1.9	±1.9	±1.0	±1.0
Pion ID	±0.5		±0.5		±0.5	
π^0 ID		±3.0		±3.0		±3.0
Fisher and $B\bar{B}$ likelihood	±1.4	±1.4	±1.7	±1.9	±1.4	±1.4
MC statistics	±0.1	±0.1	±0.1	±0.1	±0.1	±0.1
$B\bar{B}$ counting	±1.1	±1.1	±1.1	±1.1	±1.1	±1.1
Model dep.	±3.0	±3.0	±3.0	±3.0	±3.0	±3.0
signal m_{ES} model	±0.3	±5.1	±0.4	±4.9	±0.3	±5.1
signal ΔE model	±0.6	±5.1	±0.5	±5.4	±0.5	±5.2
signal ΔE radiative tail	±1.2	±1.3			±1.0	±1.4
Total	±4.9	±8.8	±5.1	±9.0	±4.9	±8.9

of the baseline fit. The uncertainty of the hadronic B decay peaking background is dominated by the control sample statistics from which it is derived; the leptonic peaking background uncertainties are dominated by the uncertainty of the assumed branching fractions for these processes, particularly $B^+ \to K^+\ell^+\ell^-$.

Figures 3 and 4 show projections onto m_{ES} and ΔE of a two-dimensional unbinned maximum-likelihood fit to measure the number of background events. The best fit PDFs are consistent with the observed data. The fit region yields for each mode are also consistent with the simulated predictions from which optimization of selection criteria were derived. We estimate the combinatorial background in the signal region from these PDFs and those estimates together with the peaking backgrounds result in about one event per decay mode expected in the signal region.

5 Results

Figure 5 shows a scatter plot of the fit region with events from the BABAR data that pass all our selection criteria. The signal events are expected to be found in the signal region marked by a box drawn in the plot. We observe a total of 3 $B \to \pi\ell^+\ell^-$ candidates and 1 $B \to \pi e\mu$ candidate in the signal region. This is consistent with no significant signal above the expected backgrounds, so we calculate upper limits at 90% confidence level via a frequentist method which takes into account uncertainties both in the signal sensitivity and in the expected background [19]. The limits are presented in Table 4, along with all numbers necessary in this method to perform the calculation. The upper limits for the electron and electron-muon modes are in the range of $1-2\times10^{-7}$; the muon modes are somewhat less sensitive with limits in the range of $2 - 5 \times 10^{-7}$. Assuming the partial widths of $B \to \pi\ell^+\ell^-$ to electrons and muons are equal, the limits for the two decay modes can be simply combined to provide a combined limit of 1.06×10^{-7} for $B^+ \to \pi^+\ell^+\ell^-$ and 1.02×10^{-7} for $B^0 \to \pi^0\ell^+\ell^-$. Assuming further that there is isospin asymmetry in the partial widths of $B \to \pi\ell^+\ell^-$ to charged and neutral pions, the four $B \to \pi\ell^+\ell^-$ modes can be combined with the constraint $\mathcal{B}(B^0 \to \pi^0\ell^+\ell^-) = \frac{1}{2} \times \tau_{B^0}/\tau_{B^+} \times \mathcal{B}(B^+ \to \pi^+\ell^+\ell^-)$ to compute a combined limit, expressed in terms of the $B^+ \to \pi^+\ell^+\ell^-$ branching fraction, of 0.79×10^{-7}. A similar combined limit of 0.98×10^{-7} is obtained for the lepton-flavor violating mode $B \to \pi e\mu$.

Table 4: Results for the $B \to \pi \ell^+ \ell^-$ analysis, including observed signal candidate events, expected background, signal yield upper limit at 90% confidence level, signal efficiency, expected branching fraction upper limit at 90% confidence level, and the observed branching fraction upper limit at 90% confidence level. The numbers in parentheses are limits evaluated without the inclusion of systematic uncertainties. Combined limits at the bottom are derived from simultaneous limits calculated from the individual modes.

Mode	Observed Events	Expected Background	Events UL 90% C.L.	Signal Efficiency	Expected BF UL 90% C.L. (10^{-7})	BF UL 90% C.L. (10^{-7})
$B^+ \to \pi^+ e^+ e^-$	1	0.96 ± 0.32	2.97 (2.93)	$7.5 \pm 0.4\%$	1.64	1.72 (1.70)
$B^0 \to \pi^0 e^+ e^-$	0	0.46 ± 0.22	1.86 (1.84)	$6.3 \pm 0.6\%$	1.79	1.29 (1.27)
$B^+ \to \pi^+ \mu^+ \mu^-$	1	0.96 ± 0.30	2.96 (2.93)	$5.2 \pm 0.3\%$	2.37	2.47 (2.45)
$B^0 \to \pi^0 \mu^+ \mu^-$	1	0.35 ± 0.19	3.57 (3.55)	$3.4 \pm 0.3\%$	3.18	4.56 (4.53)
$B^+ \to \pi^+ e\mu$	1	1.48 ± 0.48	2.49 (2.41)	$6.3 \pm 0.3\%$	2.17	1.72 (1.66)
$B^0 \to \pi^0 e\mu$	0	1.13 ± 0.47	1.28 (1.18)	$3.7 \pm 0.3\%$	3.52	1.50 (1.38)
$B^+ \to \pi^+ \ell^+ \ell^-$						1.06 (1.04)
$B^0 \to \pi^0 \ell^+ \ell^-$						1.02 (1.01)
$B \to \pi \ell^+ \ell^-$						0.79 (0.77)
$B \to \pi e\mu$						0.98 (0.90)

Table 4 also lists the mean expected upper limits, defined as a sum of upper limits obtained for n events observed ($n = 0, 1, 2...$), each weighted by the Poisson probability of observing n events when expecting background only.

6   Conclusion

We present a preliminary result of a search for $B \to \pi \ell^+ \ell^-$ using a sample of $(230.1 \pm 2.5) \times 10^6$ $B\overline{B}$ pairs produced at the $\Upsilon(4S)$ resonance. We do not see any excess of events in the signal region, and we measure the upper limit at 90% confidence level of the lepton-flavor–averaged branching fraction to be

$$\mathcal{B}(B^+ \to \pi^+ \ell^+ \ell^-) = 2 \times \frac{\tau_{B^+}}{\tau_{B^0}} \mathcal{B}(B^0 \to \pi^0 \ell^+ \ell^-) < 7.9 \times 10^{-8},$$

consistent with the Standard Model prediction of 3.3×10^{-8}. This is the first such search performed by the B factory experiments; with anticipated final samples of order 1 ab^{-1}, and with the small backgrounds observed in this analysis, it may be possible in the future to achieve an experimental sensitivity comparable to the Standard Model prediction.

7   Acknowledgments

References

[1] G. Burdman, Phys. Rev. D **52**, 6400 (1995).

[2] J. L. Hewett and J. D. Wells, Phys. Rev. D **55**, 5549 (1997).

[3] A. Ali *et al.*, Phys. Rev. D **66**, 034002 (2002).

[4] G. Eilam, J. L. Hewett, and T. G. Rizzo, Phys. Rev. D **34**, 2773 (1986); T. M. Aliev, A. Ozpineci, and M. Savci, Eur. Phys. J. C**29**, 265 (2003).

[5] S. Davidson, D. C. Bailey, and B. A. Campbell, Z. Phys. C **61**, 613 (1994).

[6] *BABAR* Collaboration, B. Aubert *et al.*, Phys. Rev. D **73**, 092001 (2006).

[7] Belle Collaboration, M. Iwasaki *et al.*, Phys. Rev. D **72**, 092005 (2005); *BABAR* Collaboration, B. Aubert *et al.*, Phys. Rev. Lett. **93**, 081802 (2004); Belle Collaboration, A. Ishikawa *et al.*, Phys. Rev. Lett. **91**, 261601 (2003).

[8] Belle Collaboration, D. Mohapatra *et al.*, Phys. Rev. Lett. **96**, 221601 (2006); *BABAR* Collaboration, B. Aubert *et al.*, Phys. Rev. Lett. **94**, 011801 (2005).

[9] Mark II Collaboration, A. J. Weir *et al.*, Phys. Rev. D **41** 1384 (1990).

[10] T. M. Aliev and M. Savci, Phys. Rev. D **60**, 014005 (1999).

[11] CLEO Collaboration, K. W. Edwards *et al.*, Phys. Rev. D **65**, 111102 (2002).

[12] *BABAR* Collaboration, B. Aubert *et al.*, Nucl. Instrum. Methods **A479**, 1-116 (2002).

[13] S. Agostinelli *et al.*, Nucl. Instrum. Methods A **506**, 250 (2003).

[14] R.A. Fisher, Ann. Eugenics **7**, 179 (1936).

[15] G.C. Fox and S. Wolfram, Phys. Rev. Lett. **41**, 1581 (1978).

[16] The i-th moment L_i is defined by $L_i = \sum_j |p_j^*||\cos(\theta_j^*)|^i$, where the p_j^* are the CM momenta of all particles not used in reconstructing the signal B candidate, and the angle θ_j^* is between the particle's momentum and the thrust axis of the signal B.

[17] W.-M. Yao *et al.* (Particle Data Group), J. Phys. G 33, 1 (2006).

[18] The function is $f(x) \propto x\sqrt{1-x^2}\exp\left[-\zeta(1-x^2)\right]$, where the slope ζ is a fit parameter and $x = m_{\mathrm{ES}}/E_{\mathrm{b}}^*$; ARGUS Collaboration, H. Albrecht *et al.*, Z. Phys. C **48**, 543 (1990).

[19] R. Barlow, Comput. Phys. Commun. **149**, 97 (2002).

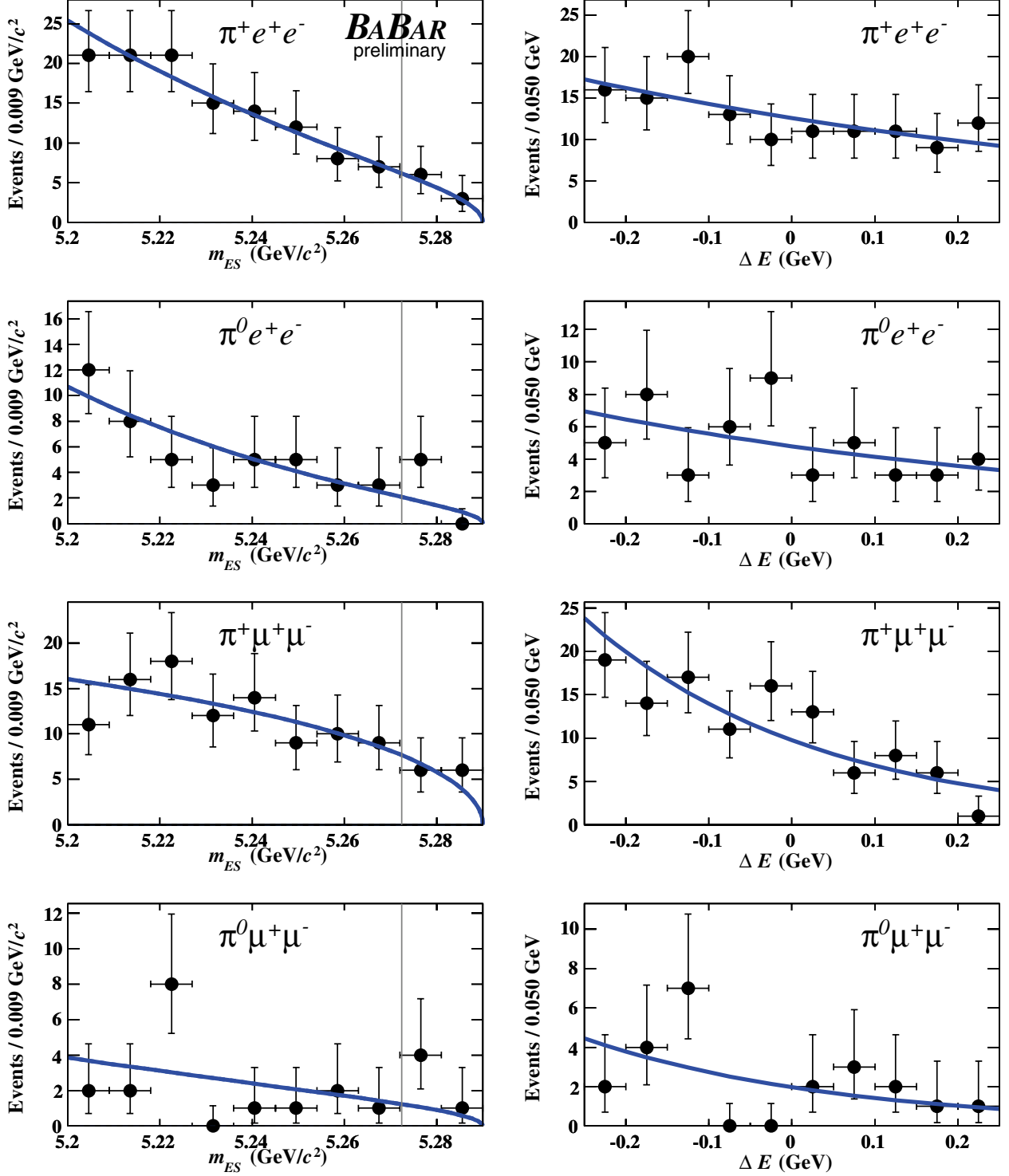Figure 3: Projections of m_{ES} and ΔE of $B \to \pi \ell^+ \ell^-$ events in the full fit region. Superimposed is the PDF we use to model combinatorial background. The parameters were obtained from two-dimensional unbinned maximum-likelihood fits to events outside the signal region, with $m_{ES} <$ 5.2724 (to the left of the gray vertical line).
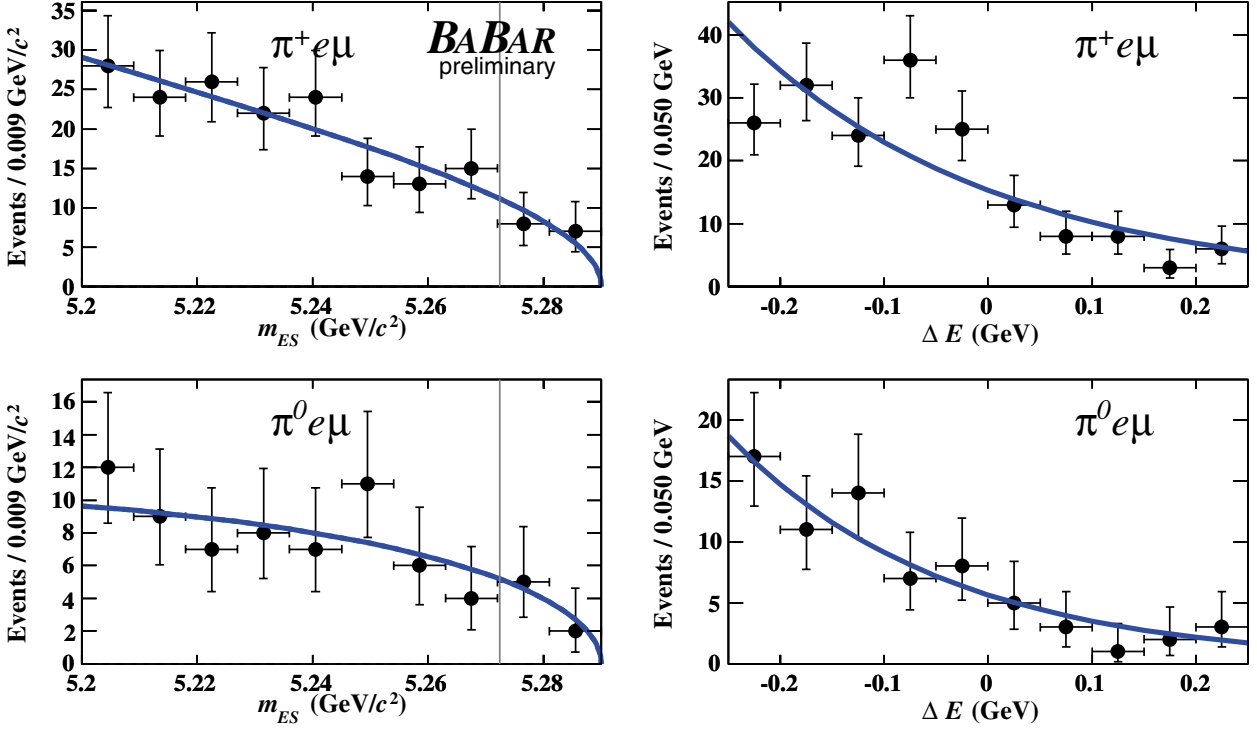
18

Figure 4: Projections of m_{ES} and ΔE of $B \to \pi e\mu$ events in the full fit region. Superimposed is the PDF we use to model combinatorial background. The parameters were obtained from two-dimensional unbinned maximum-likelihood fits to events outside the signal region with $m_{ES} <$ 5.2724 (to the left of the gray vertical line).
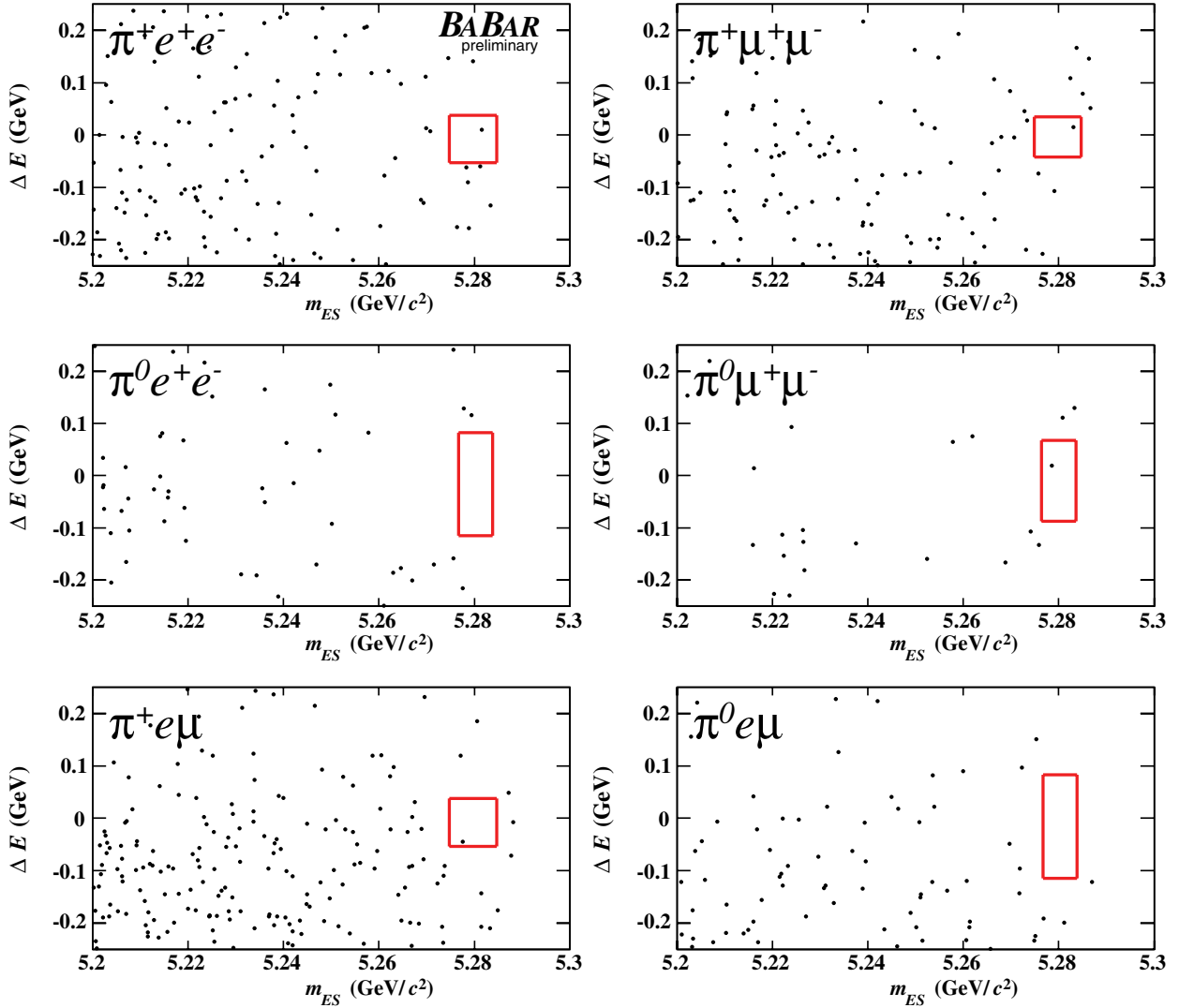
Figure 5: Distribution in two dimensions (m_{ES} and ΔE) of events in the background fit region passing the selection. The small box defines the signal region from which signal candidates are selected.